Supplementary file

1. Characterization of calcium phosphates (CaP)

1.1. Phase transformation of CaP

The purity and crystallographic phase of the synthesized calcium phosphates were verified using energy dispersive spectroscopy (EDS) and powder X-ray diffraction (XRD). The measured Ca:P atomic ratio of the brushite ($CaHPO_4 \cdot 2H_2O$) powder obtained is 1.07 ± 0.04 (**Figure S1a**). **Figure S1b** shows the phase transformation of the CaP after calcination. The synthesized brushite powder closely matched the record ICSD 16132 in the Inorganic Crystal Structure Database (ICSD). After calcination at 900°C for 6 h, the CaP obtained was verified to be β-calcium pyrophosphate ($Ca_2P_2O_7$) as its XRD spectrum closely matched the record ICSD 73712. The presence of other CaP phases was not detected.

DSC-TGA of brushite powder was performed at a heating rate of 20°C/min in air (SDT Q600, TA Instruments). **Figure S1c** shows the heat flow and mass change as brushite powder decomposes into monetite and then transforms into calcium pyrophosphate.
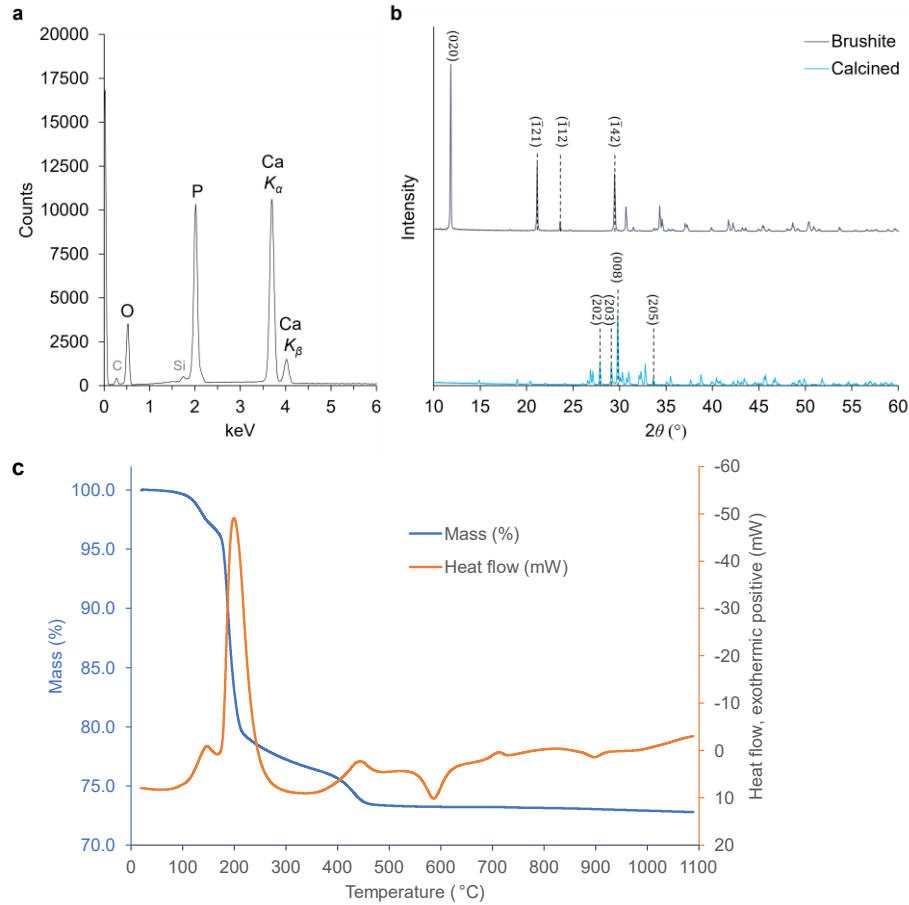
Figure S1. (a) EDS spectrum of the synthesized brushite on silicon wafer. (b) Powder XRD spectra of the synthesized brushite before (top) and after (bottom) calcination at 900°C. Peaks labeled according to ref [38]. (c) DSC-TGA of brushite powder in air.

1.2. Dimensions of synthesized brushite microplatelets in inks

The formation of the filament microstructure would not have been possible with the use of spherical or random-shaped brushite microparticles or nanoparticles. Thanks to the high aspect ratio of the brushite microplatelets, shear stresses against the nozzle wall induced preferential alignment of the anisometric particles, thereby producing the characteristic core-shell microstructure.
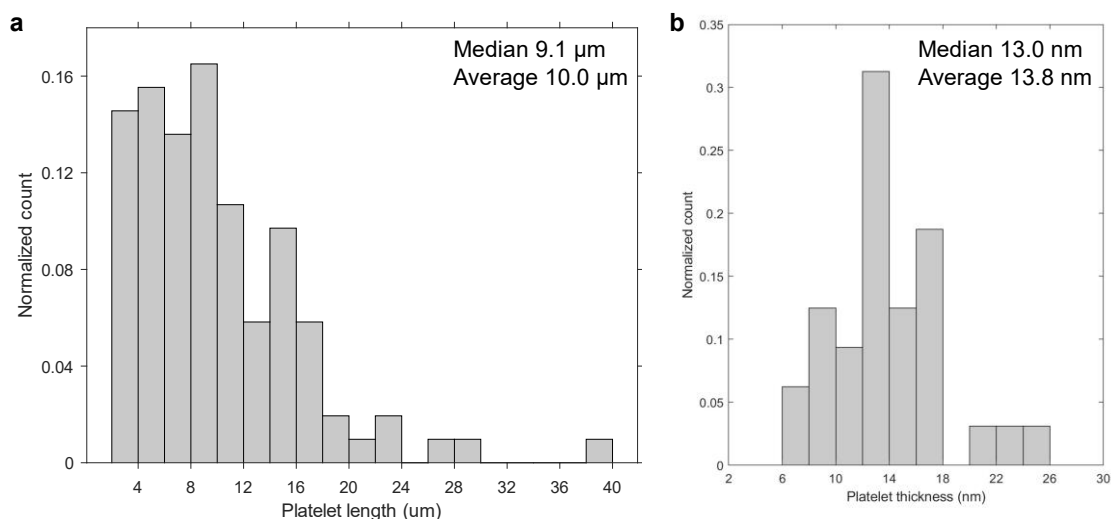
Figure S2. (a) Length and (b) thickness of synthesized brushite microplatelets, measured from scanning electron micrographs.

2. Rheological properties of brushite ink

In the absence of brushite and surfactant, the viscosity of 7 wt% PVP in water is 1.27 ± 0.15 Pa·s. As expected, the ink's zero shear viscosity increases with solid loading of brushite microplatelets (**Figure S3**). 27 vol% brushite ink appears paste-like while 21 vol% brushite ink appears liquid-like.
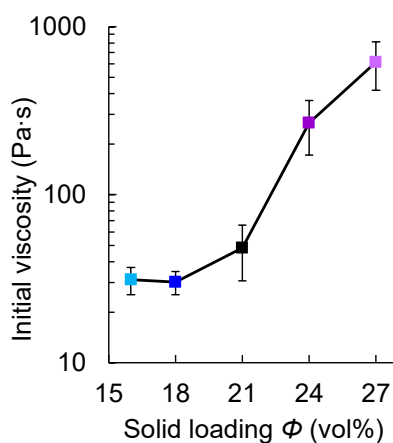

Figure S3. Zero shear viscosity of brushite inks as a function of solid loading.

3. Direct extrusion of brushite ink

3.1. Volume flow rate of ink extrusion

Given conservation of volume of an incompressible ink, the volume flow rate of ink extrusion out from the nozzle, Q, is equal to the volumetric rate of ink entering the nozzle from the syringe. In our setup as shown in Figure 1, Q is given by the plunger speed multiplied by the horizontal cross-section area of the ink barrel. The plunger speed was found to increase linearly with the nozzle diameter d, flow rate multiplier f and print speed v (**Figure S4**). Hence, the volume flow rate Q at various print parameters can be easily derived for subsequent shear rate calculations.
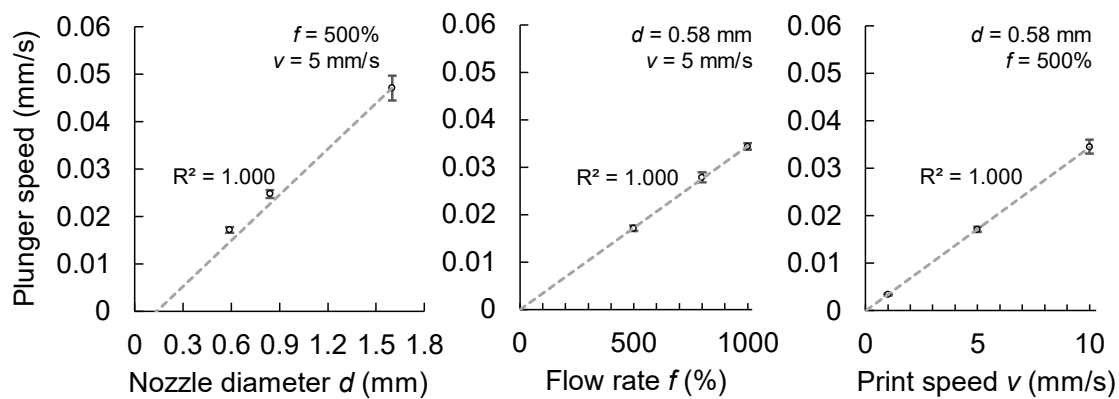

Figure S4. Plunger speed as a linear function of the print parameters d, f, and v.

3.2. Effect of nozzle size on platelet alignment

The time required for platelets to align tangentially to the nozzle wall is inversely proportional to the shear rate at the core-shell border (**Figure S5**). Furthermore, the alignment time is inversely proportional to the nozzle diameter (**Figure S5 inset**).
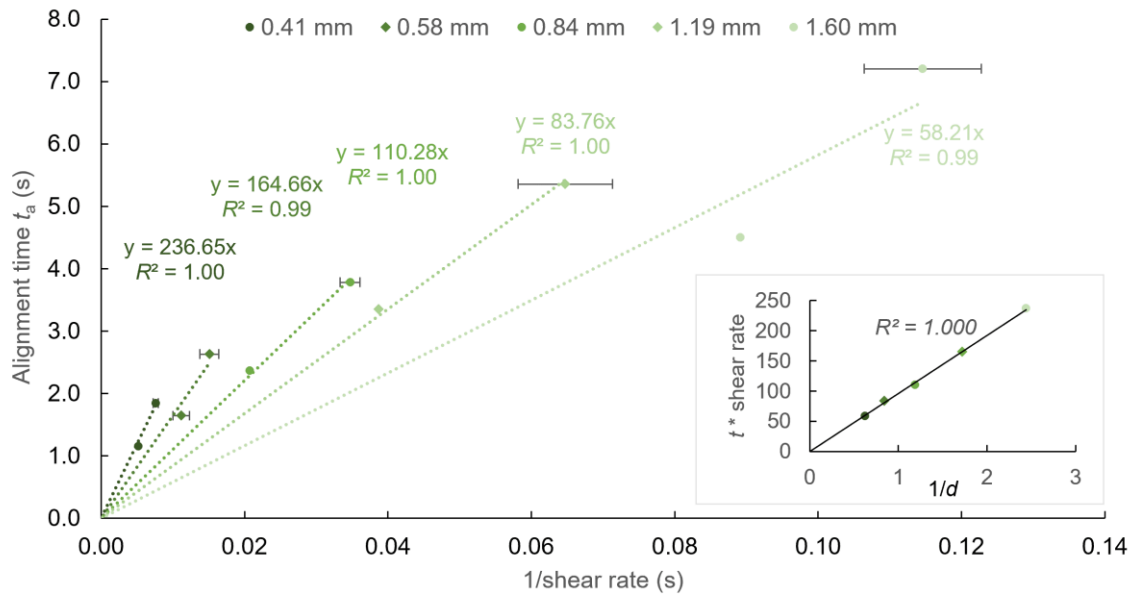
Figure S5. Alignment time as a function of the estimated shear rate at the core-shell border. Inset shows the alignment time is inversely proportional to the nozzle diameter.

The extrusion of brushite microplatelets suspended in 7% PVP down the nozzle may be modeled as laminar flow of incompressible oblate particles suspended in a Newtonian fluid down a pipe. Simulations for oblate particles based on Jeffery's orbits have predicted "log-rolling" rotational motion, "inclined" mode without rotation when wall effects dominate, or an "intermediate" state [48]. In the "inclined" mode, particles are almost tangent to the pipe wall, which could correspond to the platelets in the "shell" of our filaments [48]. The platelets at the "core" resembles the oblate particles in the "intermediate" state as the angle is typically less than 70° (**Figure 6e**).

4. Print quality of 21 vol% brushite ink

4.1. Buildability of 21 vol% brushite ink

Figure 8c shows the green brushite body with only one layer of filaments spanning over the support layers. From the follow-up buildability test with a similar print design (**Figure S6**), we can see that the brushite ink had sufficient buildability to support the weight of 4 additional layers on top even when partially unsupported beneath. Filament collapse did not occur. Future

work could quantify vertical deformation and filament sagging as well as print fidelity of small features by laser scanning confocal microscope.
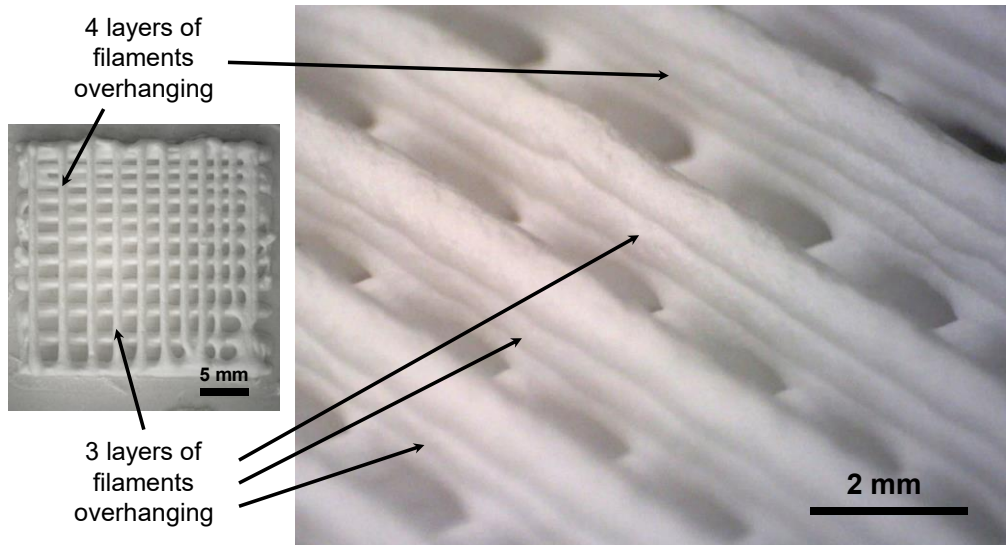

Figure S6. Brushite green body printed at $d = 0.58$ mm, $f = 500\%$, and $v = 5$ mm/s.

According to Smay *et al.* (2002) [43], the ink elasticity required to resist deformation within 5% of filament diameter is given by

$$G' \geq 1.4\rho_{\text{eff}}g\left(\frac{L}{d_{\text{filament}}}\right)^4 d_{\text{filament}} \tag{A.1}$$

where $\rho_{\text{eff}} = \rho_{\text{ink}} = 1.33$ for the specific gravity of 21 vol% brushite ink here, g is the gravitational constant, L is the center-to-center span, and d_{filament} is the filament diameter. Estimating d_{filament} as ~1000 µm in the green body for $d = 0.58$ mm and $f = 500\%$, Smay's criterion suggests a minimum G' of 1~1.5 MPa required to span across 2.8 mm. Given the G' under 0.001 MPa as shown in Figure 3c, the ability of 21 vol% brushite ink to span 2.8 mm without sacrificial supports has demonstrated a remarkable breakthrough from Smay's criterion.

4.2.Surface roughness

A 4-layer thick rectangle was printed with infill density 50%, 0.58 mm nozzle, flow rate 500%, and print speed 5 mm/s at room temperature (**Figure S7, bottom right**). The surface roughness was measured with laser scanning microscope (Keyence), giving an area roughness $R_a = 66$ µm. At the 3 white lines shown in the figure inset (**Figure S7, top right**), we obtain average line roughness of $R_z = 185$ µm and $R_a = 57$ µm. Compared to the filament width and layer height, the outer surface roughness is quite high. With reference to Figures 7a and 8d, it is no surprise that rounded filaments will produce rough surface features on the outermost top surface when closely spaced. Indeed, the individual filaments are well-defined and highly resolved across the entire surface of the rectangle.
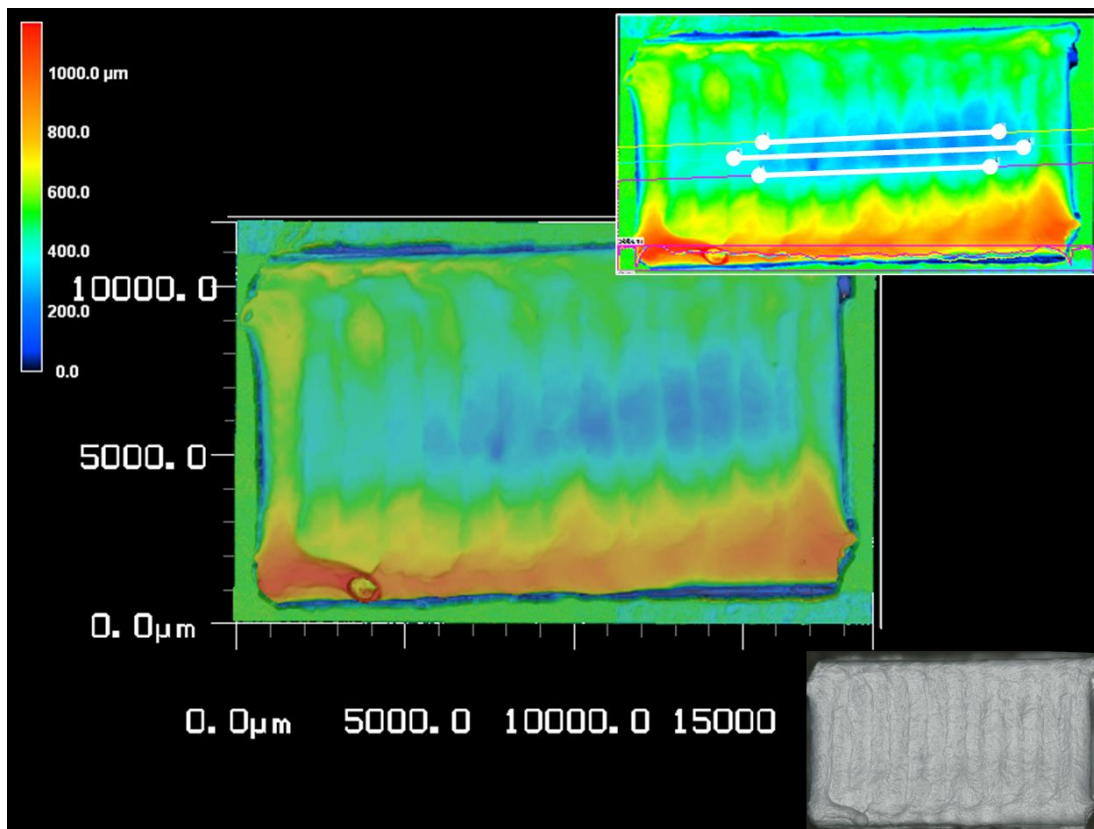

Figure S7. Topology of rectangle printed at $I_f = 50\%$, $d = 0.58$ mm, $f = 500\%$, and $v = 5$ mm/s. Top right: line roughness measurements. Bottom right: Optical scan of printed rectangle.

5. Curved crack path

The microstructure within a filament shows an orientation gradient of the microplatelets which drove cracks along unusual, curved paths (**Figure S8**).
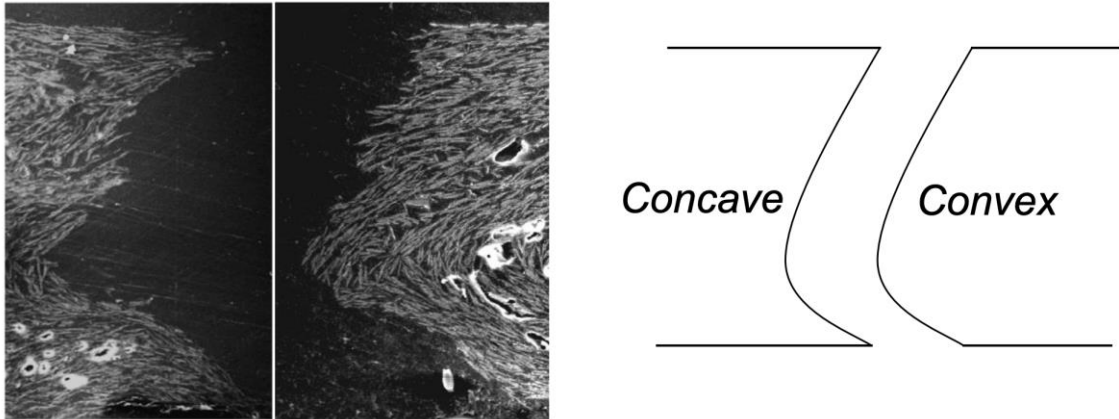

Figure S8. Polished SEM micrographs showing how curved crack path following the microplatelets plane, and schematics indicating the concave and convex fracture path.